Materials Science and Engineering C 39 (2014) 213–220

Contents lists available at ScienceDirect

Materials Science and Engineering C

journal homepage: www.elsevier.com/locate/msec

Facile synthesis of PSMA-g-3ABA/MWCNTs nanocomposite as a substrate for hemoglobin immobilization: Application to catalysis of H_2O_2

Mehdi Baghayeri [a,*], Ehsan Nazarzadeh Zare [b], Reza Hasanzadeh [c]

[a] Department of Chemistry, Faculty of Science, Hakim Sabzevari University, P.O. Box 397, Sabzevar, Iran
[b] Department of Polymer Chemistry, Faculty of Chemistry, University of Mazandaran, Babolsar, Iran
[c] Department of Chemistry, Faculty of Science, Urmia University, Urmia, Iran

ARTICLE INFO

Article history:
Received 19 November 2013
Received in revised form 19 January 2014
Accepted 1 March 2014
Available online 12 March 2014

Keywords:
Poly(styrene-alternative-maleic anhydride)
Hemoglobin
Nanocomposite
Biosensor
Electrocatalysis

ABSTRACT

The new nanocomposite films based on poly(styrene-alternative-maleic anhydride) grafted to 3-aminobenzoic acid (PSMA-g-3ABA) and multi-walled carbon nanotubes (MWCNTs) were applied to immobilize hemoglobin (Hb) for biosensor fabrication (PSMA-g-3ABA/MWCNTs). Electrochemical impedance spectroscopy was used to confirm the adsorption of Hb onto the surface of PSMA-g-3ABA/MWCNTs. The immobilized Hb maintains its bioactivities and displays an excellent electrochemical behavior. The biosensor was used to catalyze the reduction of hydrogen peroxide. The electrocatalytic response showed a linear dependence on the H_2O_2 concentration ranging widely from 1.0×10^{-6} M to 5.0×10^{-4} M with a detection limit of 3.2×10^{-7} M. The apparent Michaelis–Menten constant of Hb on the modified electrode was estimated to be 0.22 mM. The proposed method opens a way to develop biosensors by using nanostructured materials with low electrical conductivity.

1. Introduction

In recent years, there is a growing demand for rapid, reliable, and inexpensive sensors for the determination of different analytes in biomedical, environmental, and industrial samples [1–3]. Construction of electrochemical sensors using modified electrodes continues to be an area of great interest and a relatively large amount of electrochemical research has been devoted to the development and application of these sensors for the analysis of biologically active compounds [4,5]. Modification of electrodes with suitable materials facilitates the electrochemistry of the redox biological compounds, which generally results in increased selectivity and sensitivity of the determinations [6,7].

Biomolecule-immobilized sensors have found various important applications in many fields such as clinical laboratories, fermentation processes, and pollution monitoring. Within the biosensor research field, direct electron transfer between an electrode material and a redox-active protein or protein clusters has become an intriguing phenomenon for the last three decades [8]. The investigations of the direct electron-transfer process on proteins and underlying electrodes can not only help us to understand the mechanisms of redox transformations between redox biomolecules in biocatalysis and metabolic processes involving electron transportation in biological systems but also provide us a platform for fabricating biosensors, enzymatic bioreactors, and biomedical devices [9]. In general, the functions of most proteins depend upon precise three dimensional structures [10,11], which are affected by a number of noncovalent interactions such as hydrogen bonds, van der Waals interactions, electrostatic interactions, hydrophilic/hydrophobic effects, and so on [12,13]. Because of its well-known structure and commercial availability, Hb is considered as an ideal model molecule for protein electrochemistry. However, due to the deep burying of electroactive center in the protein structure, the denaturation of proteins or the unfavorable orientation on the electrode interface, it is difficult for redox proteins to achieve the direct electron transfer process on the bare electrode directly [14]. Therefore, a great amount of efforts have been devoted to the modification of either the protein or the electrode surface to limit denaturing adsorption and control the orientation at the protein/electrode interface to achieve a direct rapid electron transfer [8]. The immobilization of proteins on polymer matrices for biosensing is a promising direction given the rapid advances in biotechnology [15,16]. However, a number of polymers such as polyvinyl alcohol (PVA) with moderate molecular weight and polyvinyl pyrrolidone (PVP) have been identified as very promising immobilization matrices due to their high reaction activity for protein binding, high reproducibility, and good mechanical, thermal, and chemical stability [17–21]. On the other hand, polymer nanocomposites containing carbon nanotubes (CNTs) have been extensively explored in the recent years [22–24]. It is well known, that CNTs, used as filler in conventional polymers, can improve remarkably their mechanical and thermal properties. Moreover, when the concentration of CNTs exceeds a certain value (at which electrical percolation occurs), the electrical conductivity of the polymer composite increases over several orders of magnitude.

* Corresponding author. Tel.: +98 5714003325; fax: +98 5714003170.
E-mail address: m.baghayeri@hsu.ac.ir (M. Baghayeri).

http://dx.doi.org/10.1016/j.msec.2014.03.012
0928-4931/

These conductive, flexible and easy processable thermoplastic materials can find a lot of applications in electronics and medicine as smart materials. In particular, when a CNT/polymer composite responds to certain external stimuli with an electrical resistance change, it may be used as a sensor [25–27]. The presence of multi-walled carbon nanotubes (MWCNTs) provides a stage for the interactions of biomolecules and polymer chains, changes the morphology, increases the loading of biomolecules, improves the permeability and the conductivity of the polymer film, and accelerates the electron transfer of the immobilized redox agents through the conducting tunnels of MWCNTs [28]. Up to date, many studies have been reported on sensing properties of immobilized Hb on the CNT/polymer composites. Liu et al. have studied the direct electron-transfer reactivity of immobilized hemoglobin on a polyurethane elastomer (PUE) film mixed with MWCNTs [28]. Wen et al. reported direct electrochemistry and electrocatalysis of hemoglobin immobilized in poly(ethylene glycol) grafted multi-walled carbon nanotubes [29]. Wang et al. applied a new composite film composed of diblock weak polyelectrolyte poly(2-hydroxyethyl methacrylate)-b-poly(2-(dimethylamino) ethyl methacrylate) and MWCNTs to immobilize hemoglobin for biosensor fabrication [30]. A prerequisite for applying these sensors is the appropriate immobilization of Hb on biocompatible beds. Such biocompatible surfaces can often be used for various purposes in bio-related applications [31–33]. In recently reported works, biocompatible poly(styrene-alt-maleic acid) (PSMAC) and modified poly(styrene-alt-maleic anhydride) (PSMA) copolymers have been introduced as external dopant, drug carriers and excellent sorbent for removal of heavy metals [34–40]. In this paper, PSMA-*g*-3ABA/MWCNTs nanocomposite was employed as a conducting matrix to immobilize Hb and promote direct electrochemistry of protein on the electrode surface. To the best of our knowledge, this is the first attempt to use a PSMA-*g*-3ABA/MWCNTs nanocomposite as a biosensor matrix and the investigation of their hydrogen peroxide sensing characteristics. Such unique structure of the PSMA-*g*-3ABA prevents the leakage of the Hb and leads to good preparation reproducibility for the sensor. On the other hand, the presence of MWCNTs provides a unique three-dimensional netlike porous structure for the interaction of Hb and PSMA-*g*-3ABA. The prepared biosensor for hydrogen peroxide shows good analytical performance, indicating that the PSMA-*g*-3ABA/MWCNTs matrix is a sort of biomaterial suitable for Hb immobilization and preparation of biosensors.

2. Experimental section

2.1. Materials and apparatus

Styrene, C_8H_8, (Merck) was purified by distillation at reduced pressure. Maleic anhydride (MA, $C_4H_2O_3$), triethylamine (TEA, $N(CH_2CH_3)_3$), 3-aminobenzoic acid (3ABA, $C_7H_7NO_2$), tetrahydrofuran (THF, C_4H_8O), hydrochloric acid (HCl), sodium hydroxide (NaOH) and benzoyl peroxide (BPO, $C_{14}H_{10}O_4$) were purchased from Merck and was used without further purification. Hemoglobin from bovine blood (Sigma-Aldrich) was used without further purification. MWCNTs (>95%, O.D.: 10–15 nm, I.D.: 2–6 nm, length: 0.1–10 μm) were purchased from Sigma-Aldrich. MWCNTs were chemically functionalized by ultrasonication in a mixture of sulfuric acid and nitric acid (3:1 v/v) for 8 h. Then, functionalized MWCNTs were washed with deionized water and separated by centrifuging three times. The carboxylic groups of functionalized MWCNTs were confirmed by FT-IR with stretching bands of carboxylic acid groups at 1710 cm^{-1} [41]. High viscosity paraffin (density = 0.88 g cm^{-3}) from Fluka was used as the pasting liquid. Hydrogen peroxide (H_2O_2) solutions (from Sigma-Aldrich) were freshly prepared before being used. Phosphate buffer solutions (PBS) were prepared with sodium phosphate dibasic (Na_2HPO_4) and sodium phosphate monobasic NaH_2PO_4 from Fluka. All other chemicals were of analytical grades and were used without further purification. All solutions were prepared with double-distilled water.

Cyclic voltammetry (CV) and electrochemical impedance spectroscopy (EIS) measurements were carried out on an Autolab potentiostat/galvanostat (Eco Chemie BV, Netherlands) with data acquisition software, made available by the manufacturer (GPES and FRA 4.9 version). An Ag|AgCl|KCl (3.0 M) electrode and a platinum electrode were used as the reference and counter electrode, respectively. A digital pH-meter (780 pH meter, metrohm) with precision of ±0.001 was used to read the pH value of the buffer solutions. Electrolyte solutions were deoxygenated by purging pure nitrogen (99.99%) for 10 min prior to electrochemical experiments. All measurements were carried out under a nitrogen atmosphere. A Philips model XL30 scanning electron microscope (SEM) was used to determine the morphology of nanoparticles. FT-IR spectra were recorded on a Bruker Tensor 27 spectrometer (Bruker, Karlsruhe, Germany). All experiments were performed at room temperature (25 ± 2 °C). Thermogravimetric analysis (TGA) of prepared polymers was determined using the LENSES STAPT-1000 calorimeter (Linseis STAPT1000, Selb, Germany) by scanning up to 1000 °C with the heating rate of 10 °C/min.

2.2. Synthesis of PSMA-g-3ABA

PSMA was synthesized through the thermally initiated free-radical polymerization of styrene and maleic anhydride with benzoyl peroxide (BPO) as an initiator [35]. Also, the modified PSMA copolymer was successfully prepared by the chemical graft reaction of 3ABA on PSMA as described in reported lecture [38]. Briefly, 3 g (0.015 mol) PSMA copolymer and 1.03 g (0.008 mol) 3ABA in molar ratio of 1:0.5 were poured into a flask. Then, 0.5 mL (0.004 mol) of triethylamine (TEA) and 50 mL THF were added. The reaction mixture was refluxed for 5 h under inert atmosphere. Then the reaction was cooled to room temperature and finally precipitation was accomplished by adding n-hexane as non-solvent. Finally, the obtained precipitate was filtrated and washed with n-hexane several times. The product was dried in vacuum oven for 48 h in 70 °C (yield 95%) and named PSMA-*g*-3ABA.

2.3. Preparation of PSMA-g-3ABA/MWCNTs nanocomposite and preparation of modified electrode

The PSMA-*g*-3ABA (0.5 g) was added to 20 mL of THF and stirred at room temperature until complete dissolution. Afterward, MWCNTs (0.5 g) were added to the aforementioned solution and stirred overnight at room temperature to form a homogeneous suspension. Additional coating formulations were prepared with different amounts of PSMA-*g*-3ABA and different ratios of MWCNTs. The coating solutions were cast on a glass matrix. After being dried at room temperature for 24 h, homogenous nanocomposite was obtained.

The working electrode was prepared as follows: 80 mg of graphite powder, 20 mg of PSMA-*g*-3ABA/MWCNTs nanocomposite and 12 μL of paraffin oil were mixed by hand to produce a homogeneous carbon paste. The carbon paste was packed into the cave of a homemade carbon paste electrode and then smoothed on a weighing paper. Then, the electrode was immersed into the Hb solution (10 mg/mL in pH 7.0 PBS) for 80 min and named Hb-PSMA-*g*-3ABA/MWCNTs/CPE. The Hb-PSMA-*g*-3ABA/MWCNTs/CPE was also thoroughly rinsed with water to remove the unabsorbed Hb molecules and was dried in air. The Hb-MWCNTs/CPE, Hb-PSMA-*g*-3ABA/CPE and Hb-CPE were also prepared in the above manner described for comparison and stored at 4 °C in a 0.1 M PBS (pH 7.0) when not in use.

3. Results and discussion

3.1. Characterization of Hb immobilized on PSMA-g-3ABA/MWCNTs/CPE

The free-radical polymerization of PSMA was facile and the copolymer was readily recovered. Styrene and maleic anhydride are known to produce alternating copolymers, and the molecular weight of the

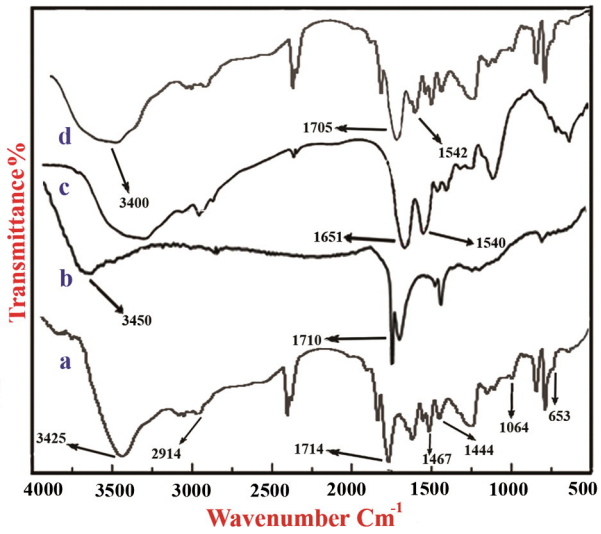

Fig. 1. FT-IR spectra of PSMA-*g*-3ABA (a), MWCNTs (b), Hb (c) and Hb-PSMA-*g*-3ABA/MWCNTs (d).

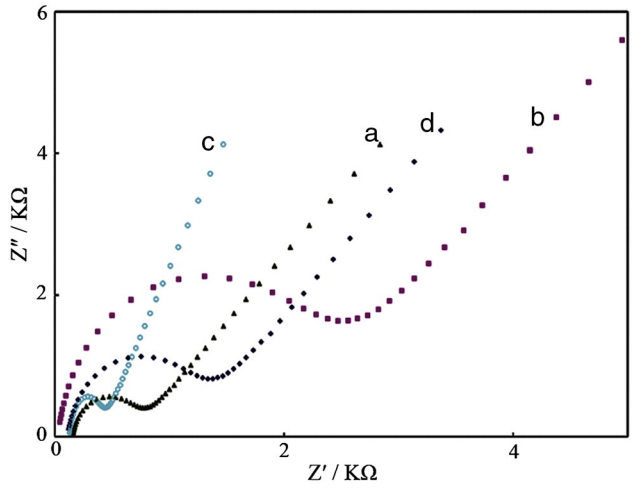

Fig. 3. The AC impedance spectra of the PSMA-*g*-3ABA/CPE (a), Hb-PSMA-*g*-3ABA/CPE (b), PSMA-*g*-3ABA/MWCNTs/CPE (c) and Hb-PSMA-*g*-3ABA/MWCNTs/CPE (d), recorded at the open circuit potential in 0.1 M PBS (pH 7.0) containing 0.1 M $K_3Fe(CN)_6$ and 0.1 M $K_4Fe(CN)_6$.

copolymers could be controlled by variation of the molar ratio of the free-radical initiator to the volume of added solvent. The PSMA-*g*-3ABA was prepared by amidation anhydride moieties of the PSMA copolymer. The amine group of 3ABA reacts with maleic anhydride repeated groups in the PSMA copolymer backbone to form an alkylamide linkage and a carboxylic acid group. Amide bonds are significantly resistant to hydrolysis, so the resulting copolymer will be stable in the acidic and basic medium.

The FT-IR spectra of PSMA-*g*-3ABA (a), MWCNTs (b), Hb (c) and Hb-PSMA-*g*-3ABA/MWCNTs (d) are presented in Fig. 1. The spectral feature of PSMAC copolymer is also well demonstrated in our previous literature [35]. As shown in Fig. 1a, a broad peak around 3425 cm^{-1} can be assigned to the stretching vibration of acidic OH and amidic NH of PSMA-*g*-3ABA. The observed peak at 2914 cm^{-1} is assigned to aliphatic C–H stretching vibration. The peaks at 1714 cm^{-1} can be assigned to vibration of acidic and amidic carbonyl groups, which is overlapped. The peaks at 1467 cm^{-1} and 1444 cm^{-1} correspond to stretching vibration of C–O and C–N bonds conjugated with aromatic rings. Also the peaks at 1064 cm^{-1} and 653 cm^{-1} correspond to C–N and N–H stretching vibrations. As can be seen from Fig. 1b, the absorption bands at 3450 cm^{-1} and 1710 cm^{-1} correspond to the stretching vibration of O–H and carbonyl of carboxylic acid. As shown in Fig. 1c, the strong broad band around 1651 cm^{-1} resulted from carbonyl stretching vibration of the peptide linkages in the Hb backbone. Meanwhile the peak at 1540 cm^{-1} is assigned to the combination of N–H bending and C–N stretching in Hb. The absorption bands of Hb-PSMA-*g*-3ABA/MWCNTs nanocomposite situating around 1542 cm^{-1} and 1705 cm^{-1} were attributed to the C–N and C═O stretching vibrations, respectively. The shift of the absorption band around 1705 cm^{-1} can be attributed to the interaction between Hb, PSMA-*g*-3ABA and MWCNTs. On the other hand, the shift around 1542 cm^{-1} is related to blue-shifting. These absorption bands confirm the successful formation of Hb-PSMA-*g*-3ABA/MWCNTs nanocomposite.

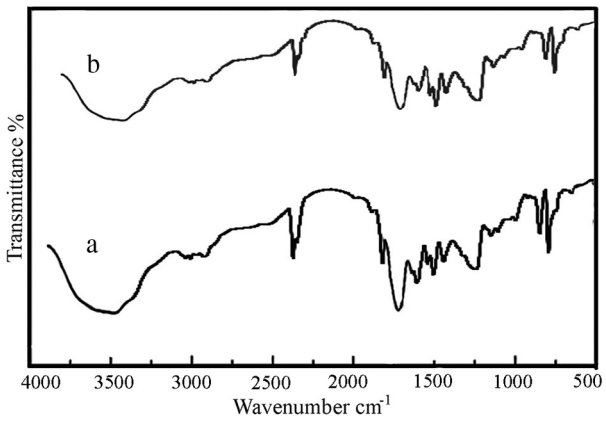

Fig. 2. FT-IR spectra of Hb-PSMA-*g*-3ABA/MWCNTs before (a) and after (b) catalytic reaction.

Fig. 2 shows the FT-IR spectra of the Hb-PSMA-*g*-3ABA/MWCNTs nanocomposite before (curve a) and after (curve b) the catalytic reaction. As can be seen from curves a and b, there is no obvious change in FT-IR spectra of the Hb-PSMA-*g*-3ABA/MWCNTs before and after the catalytic reaction. This result suggests that Hb in the Hb-PSMA-*g*-3ABA/MWCNTs retains its stability.

The electrochemistry and the response to the electrochemical probe of the PSMA-*g*-3ABA are checked by CV and EIS. The CV of PSMA-*g*-3ABA/CPE gives a low charge current, and no clearly formed peaks can be seen in the potential range from 0.5 to −0.5 V in 0.1 M PBS, pH 7.0 (not shown). Fig. 3 exhibits the electrochemical impedance spectra of different modified electrodes. The electron transfer resistance (R_{et}) at the electrode surface can be used to describe the interface properties of the electrode, which is equal to the semicircle diameter of electrochemical impedance spectra [42,43]. For electrochemical impedance spectrum of bare CPE (curve a), the semicircle domain of it is very small (R_{et} = 800 Ω), which indicated very low electron transfer resistance to the redox-probe dissolved in the electrolyte solution. However, the R_{et} (2650 Ω, curve b) of the PSMA-*g*-3ABA/CPE is much larger than that of the bare CPE. It is implied that PSMA-*g*-3ABA copolymer in the electrode surface can inhibit the electron transfer of the redox-probe of $[Fe(CN)_6]^{3-/4-}$ to the electrode surface to a certain degree. After added MWCNTs, the R_{et} of PSMA-*g*-3ABA/MWCNTs/CPE decreases to about 450 Ω (curve c), indicating that MWCNTs have good conductivity and the PSMA-*g*-3ABA/MWCNTs can make the electron transfer easier. However, the R_{et} of Hb-PSMA-*g*-3ABA/MWCNTs/CPE increases to 1380 Ω (curve d). It is indicated that the Hb was immobilized steadily into the PSMA-*g*-3ABA/MWCNTs/CPE. These data suggest that MWCNTs help to increase the electron transfer rate.

Upon addition of Hb to the PSMA-*g*-3ABA solution in THF, the transparent solution becomes cloudy due to the aggregation of Hb and copolymer (not shown). This observation is the same with other reported

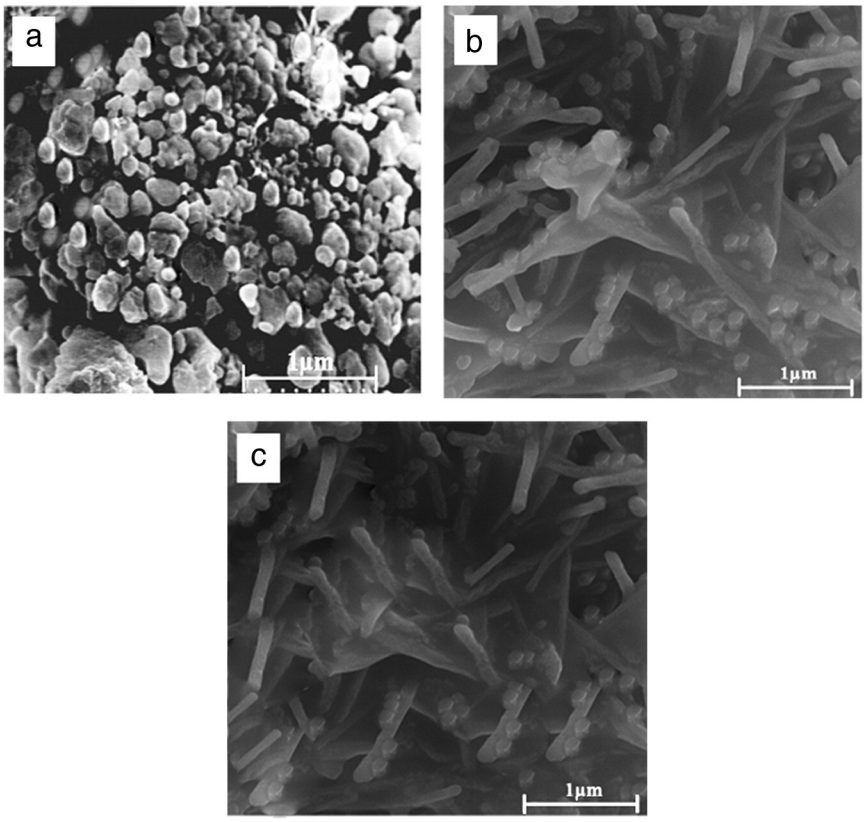

Fig. 4. The SEM images of PSMA-*g*-3ABA (a) and Hb-PSMA-*g*-3ABA/MWCNTs/CPE before (b) and after (c) catalytic reaction.

papers about addition of protein to a nonconducting polymer matrix, suggesting a strong interaction between copolymer and Hb [34,44].

The SEM morphologies of PSMA-*g*-3ABA (a) and Hb-PSMA-*g*-3ABA/MWCNTs before (b) and after (c) the catalytic reaction were compared (Fig. 4). As it can be seen in Fig. 4a, the top view of PSMA-*g*-3ABA film reveals a three-dimensional porous structure aggregated as globular particles (diameter <1 μM). In contrast, uniform and well distributed aggregates of PSMA-*g*-3ABA were observed on the Hb-PSMA-*g*-3ABA/MWCNTs which provide a high surface-to-volume ratio and enhance the electron transfer kinetics between the Hb and electrode surface (Fig. 4b). The interaction between copolymer and protein might cause a change in the protein conformation, increases the protein flexibility, and finally results in the aggregation of the copolymer with the protein [45]. The SEM morphology of Hb-PSMA-*g*-3ABA/MWCNTs after the catalytic reaction was rather similar compared to that of the Hb-PSMA-*g*-3ABA/MWCNTs before the catalytic reaction, which can be assigned to the stability of biosensor.

Fig. 5 shows the comparative thermogravimetric analysis curves of Hb-CPE (a), Hb-MWCNTs/CPE (b), Hb-PSMA-*g*-3ABA/CPE (c) and Hb-PSMA-*g*-3ABA/MWCNTs/CPE (d) under nitrogen atmosphere at the heating rate of 10 °C/min. As shown in Fig. 5a, the thermal decomposition of Hb-CPE took place mainly at 360 °C (weight loss 1.25%) that could be ascribed to the decomposition of Hb [46]. Hb-MWCNTs/CPE (Fig. 5b) showed weight loss 3.5% at 100–850 °C which could be related

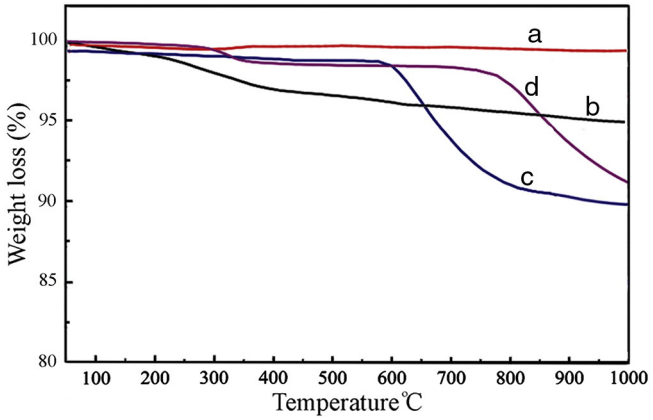

Fig. 5. TGA curves of Hb-CPE (a), Hb-MWCNTs/CPE (b), Hb-PSMA-*g*-3ABA/CPE (c) and Hb-PSMA-*g*-3ABA/MWCNTs/CPE (d). Measurements were performed under nitrogen atmosphere at the heating rate of 10 °C/min.

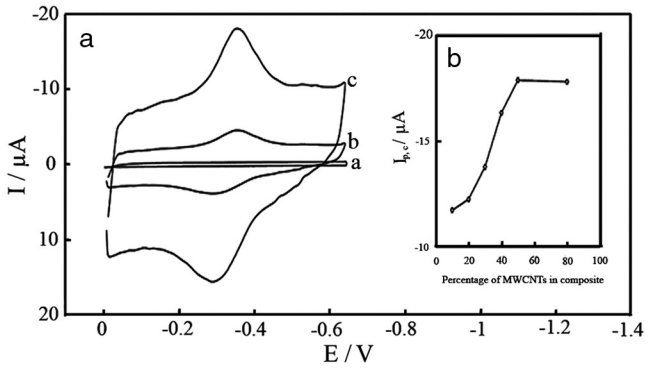

Fig. 6. (A) CVs of PSMA-*g*-3ABA/MWCNTs/CPE (a), Hb-MWCNTs/CPE (b) and Hb-PSMA-*g*-3ABA/MWCNTs/CPE (c) in 0.1 M PBS (pH 7.0) saturated with N_2 at a scan rate of 0.1 V s^{-1}. (B) Effect of the MWCNTs content in nanocomposite on the current response of the Hb-PSMA-*g*-3ABA/MWCNTs/CPE.

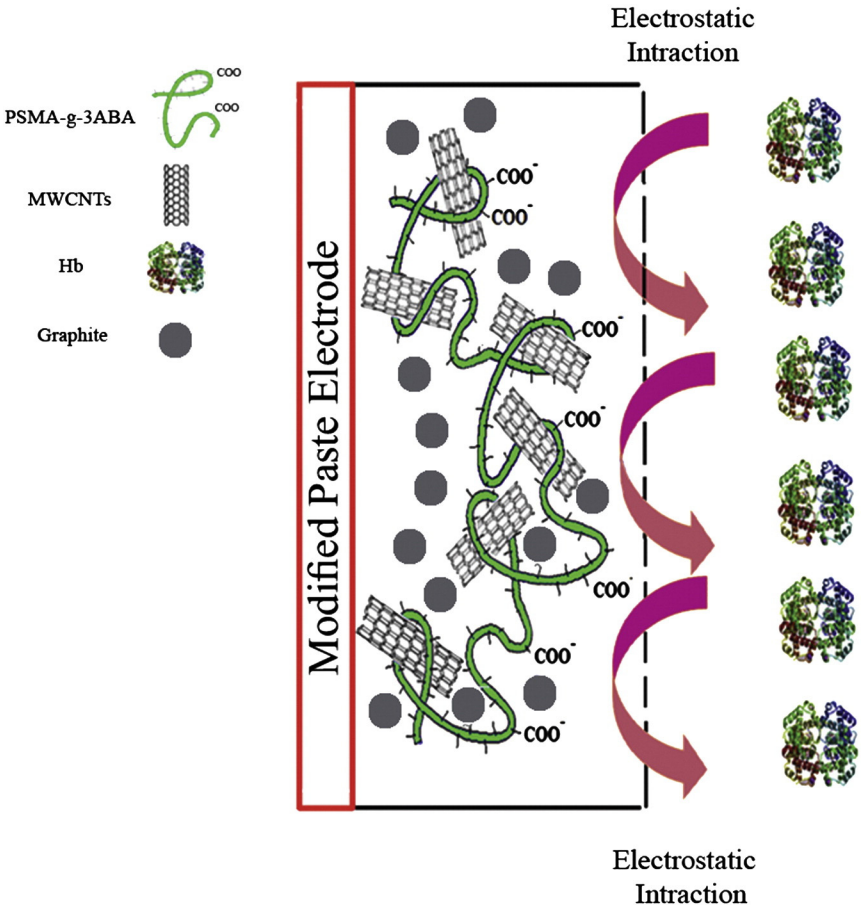

Scheme 1. The electrode construction pathway and the possible interaction between MWCNTs, PSMA-*g*-3ABA and Hb in the preparation of Hb-PSMA-*g*-3ABA/MWCNTs/CPE.

to decomposition of evaporation of moisture, Hb and carboxyl groups on the surface of MWCNTs groups [47]. In TGA curve of Hb-PSMA-*g*-3ABA/CPE (Fig. 5c), the weight loss 9% between 50 °C and 850 °C can be attributed to the evaporation of moisture, decomposition of Hb, formation of acid anhydride from the carboxyl groups with loss of water and decomposition of aromatic groups [38]. Fig. 5d demonstrated that the thermal stability of Hb-PSMA-*g*-3ABA/MWCNTs/CPE is higher than that of Hb-PSMA-*g*-3ABA/CPE which can be ascribed to interaction between Hb and PSMA-*g*-3ABA/MWCNTs.

3.2. Electrochemical behaviors of Hb

The electrochemical properties of Hb on the PSMA-*g*-3ABA/MWCNTs modified electrodes were examined. Fig. 6A shows the typical CVs of the PSMA-*g*-3ABA/MWCNTs/CPE and Hb-PSMA-*g*-3ABA/MWCNTs/CPE in 0.1 M PBS (pH 7.0) at a scan rate of 0.1 V s^{-1}. No redox peak was observed for the PSMA-*g*-3ABA/MWCNTs/CPE (Fig. 6A, curve a), indicating that PSMA-*g*-3ABA/MWCNTs are electroinactive within the potential window. However, the Hb-PSMA-*g*-

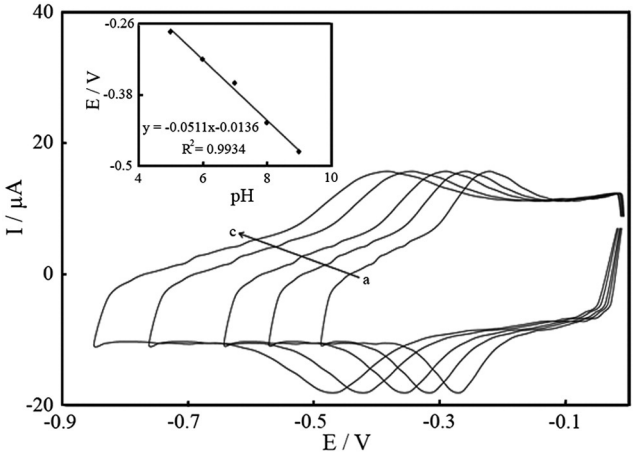

Fig. 7. CVs of Hb-PSMA-*g*-3ABA/MWCNTs/CPE in 0.1 M PBS with different pH values of 5.0 (a), 6.0 (b), 7.0 (c), 8.0 (d) and 9.0 (e) at a scan rate of 0.1 V s^{-1}. Inset: relationship for formal potentials of Hb-PSMA-*g*-3ABA/MWCNTs/CPE with pH.

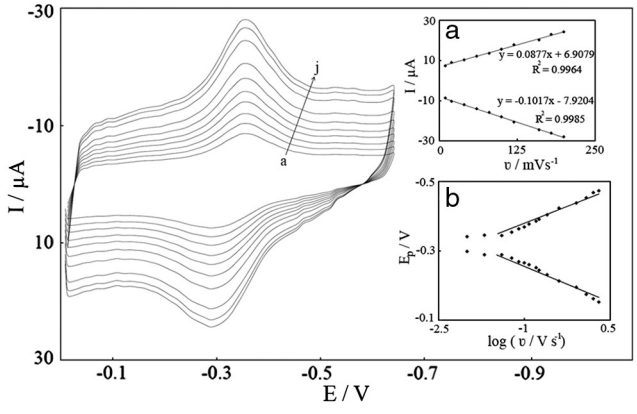

Fig. 8. CVs of Hb-PSMA-*g*-3ABA/MWCNTs/CPE in 0.1 M PBS (pH 7.0) at scan rates of 10 (a), 20 (b), 40 (c), 60 (d), 80 (e), 100 (f), 120 (g), 160 (h), 180 (i) and 200 (g) mV s^{-1}. Inset a: plot of peak current vs. scan rate. Inset b: relationship of the anodic and cathodic peak potential against log *υ*.

3ABA/MWCNTs/CPE displayed a couple of stable and well-defined redox peaks at about −0.36 and −0.28 V vs. Ag|AgCl|KCl (3.0 M), respectively (Fig. 6A, curve c). The formal potential ($E^{0'}$, the average value of the anodic and cathodic peak potentials) was around −0.32 V vs. Ag|AgCl|KCl (3.0 M), which was similar to those of −0.343 V with Nafio–Hb–CNT [48], −0.34 V with Hb-poly(ethylene glycol)-MWCNTs [49], and −0.35 V with Hb–gelatin–CNT [50], suggesting that most molecules retained their native structure after immobilization on the PSMA-*g*-3ABA/MWCNTs matrix. In comparison, we find that the peak currents obtained at the Hb-PSMA-*g*-3ABA/MWCNTs/CPE are remarkably larger than that obtained at the Hb-MWCNTs/CPE (Fig. 6A, curve b), suggesting that it is relatively difficult to realize the direct electron transfer of the Hb at the pristine MWCNTs, which coincides with the previous reports [50,51]. The results demonstrated that with the benefits of the unique properties such as high surface area and good electrical conductivity of MWCNTs as well as the biocompatibility of PSMA-*g*-3ABA (with nanostructure), the PSMA-*g*-3ABA/MWCNTs could facilitate the direct electron transfer between the Hb and the electrode more effectively.

Fig. 6B shows the dependence of the current response of the Hb-PSMA-*g*-3ABA/MWCNTs/CPE in 0.1 M PBS (pH 7.0) on the amount of MWCNTs in nanocomposite (from 10 to 80% (w/w)). The anodic and cathodic peak currents gradually increase with the increasing concentration of the MWCNTs, indicating that the MWCNTs facilitate electron transfer between Hb and the electrode [28]. For Hb-PSMA-*g*-3ABA/MWCNTs/CPE, the peak current reached the steady state after several CV cycles in buffers. Thus, all of the voltammetric experiments with Hb-PSMA-*g*-3ABA/MWCNTs/CPE were conducted at their steady states. The electrode construction pathway and the possible interaction between MWCNTs, PSMA-*g*-3ABA and Hb in the formation of modified electrode are given in Scheme 1. The pH effect on the electrochemistry of Hb was examined. The results show that the electrode potential of the redox peak strongly depends on the pH of the electrolytes (Fig. 7). Increasing the pH of the electrolyte (from 5.0 to 9.0) results in a linear negative shift of the formal potential with a slope of $-(0.0511 \pm 1.2)$ V pH^{-1} (Fig. 7, inset), which is smaller than the theoretical value of -0.059 V pH^{-1} for reversible single electron transfer coupled with proton [52]. The electron transfer between Hb and the electrode could be expressed as follows: $Hb/Fe(III) + H^+ + e^- = Hb/Fe(II)$. The fact that the slope value is smaller than -0.059 V pH^{-1} is probably because of the influence of the protonation states of trans ligands to the heme iron and amino acids around the heme, or the protonation of the water molecule coordinated to the central iron [53,54].

3.3. Effect of potential scan rate

The cyclic voltammograms of Hb-PSMA-*g*-3ABA/MWCNTs/CPE in 0.1 M PBS (pH 7.0) at different scan rates was studied in Fig. 8. When the scan rate increased, the redox peak currents (i_p) of the adsorbed Hb increased, accompanied by a slightly enlarged peak-to-peak separation (ΔE_p). The anodic and cathodic peak currents were linearly related to the scan rate in the range of 0.01–0.2 V s^{-1} with regression coefficients of 0.9964 and 0.9985, respectively (inset a in Fig. 8). This indicates that the electron transfer process of Hb-PSMA-*g*-3ABA/MWCNTs/CPE is surface controlled. The apparent heterogeneous electron transfer rate constant (k_s) for Hb-PSMA-*g*-3ABA/MWCNTs/CPE was estimated by cyclic voltammetry with Laviron's method [52] of the following equations:

$$E_{pc} = E^{\circ'} - (2.3RT/\alpha nF)\log\upsilon \quad (1)$$

$$E_{pa} = E^{\circ'} + (2.3RT/(1-\alpha)nF)\log\upsilon \quad (2)$$

$$\log k_s = \alpha\log(1-\alpha) + (1-\alpha)\log\alpha - \log(RT/nF\upsilon) - (1-\alpha)\alpha F\Delta E_p/2.3RT \quad (3)$$

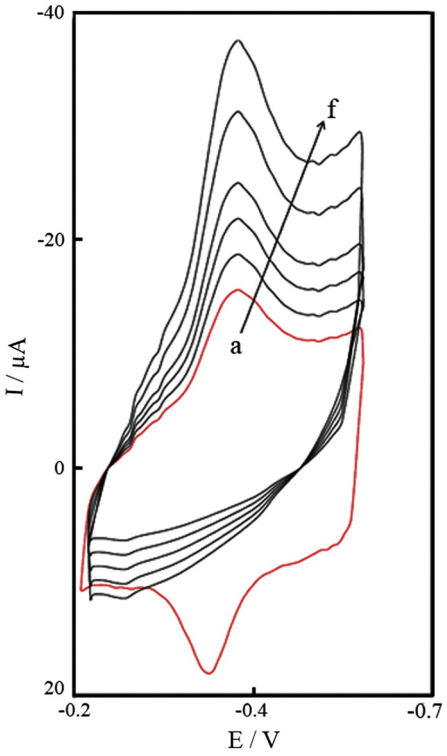

Fig. 9. CVs of Hb-PSMA-*g*-3ABA/MWCNTs/CPE in 0.1 M PBS (pH 7.0) containing different concentrations of H_2O_2 0.0 (a), 30.0 (b), 40.0 (c), 60.0 (d), 80.0 (e) and 100.0 (f) μM at a scan rate of 0.1 V s^{-1}.

where R is the charge transfer coefficient and *n* is the number of electrons transferred. The relationships of peak potentials with log υ were shown in inset b of Fig. 8. According to Eqs. (1) and (2), the charge transfer coefficient (α) can be calculated and the result found was 0.5. The heterogeneous electron transfer rate constant (k_s) was further calculated from the relationship of ΔE_p with log υ on the basis of Eq. (3), and the result was 0.92 s^{-1}. This value is larger than those of 0.58 s^{-1} for Hb entrapped in carbon nanotube [55] and 0.4 s^{-1} on the polymer–Hb–DMWCNT composite film [56], which implies that PSMA-*g*-3ABA must play a key role in promoting the direct electrochemistry of Hb in the modified electrode.

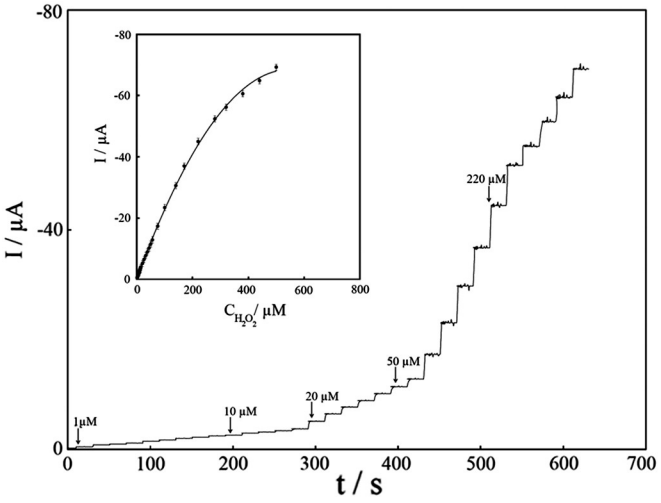

Fig. 10. Amperometric response of the H_2O_2 biosensor to successive addition of different concentration of H_2O_2 in 0.1 M PBS (pH 7.0) at the working potential of −0.4 V. Inset: plot of electrocatalytic peak current vs. concentration of H_2O_2.

From the integration of the Fe (III) reduction peaks of Hb-PSMA-*g*-3ABA/MWCNTs/CPE at different scan rates and according to Faraday's law $Q = nFA\Gamma^*$ (where n is the electron-transfer number, F is Faraday's constant, and A is the geometrical surface area of electrode), the surface concentration (Γ^*) of the electroactive Hb in the Hb-PSMA-*g*-3ABA/MWCNTs/CPE was estimated to be 2.8×10^{-9} mol cm^{-2}. This value is larger than those of $(5.0 \pm 0.3) \times 10^{-10}$ mol cm^{-2} on Hb/grafted collagen-MWCNTs [57], $(5.74 \pm 0.57) \times 10^{-12}$ mol cm^{-2} on Nafion–Hb–CNTs [58], 2.93×10^{-11} mol cm^{-2} on Hb-agarose hydrogel [59], and 4.34×10^{-10} mol cm^{-2} on Hb–gelatin–CNTs [50], indicating saturated protein adsorption and the high protein loading ability of the PSMA-*g*-3ABA/MWCNTs.

The Hb-PSMA-*g*-3ABA/MWCNTs/CPE was stored at 4 °C, and the stability was investigated by measuring the cyclic voltammogram periodically. The results indicated that the peak potentials and currents of Hb-PSMA-*g*-3ABA/MWCNTs/CPE were stable for two weeks and then decreased gradually. Also, the cyclic voltammetric peak potentials appeared at the same position with the peak current decreased 20% compared with the initial response after 1 month.

3.4. Electrocatalytic reactivity of modified electrode

The electrocatalytic activity of the Hb-PSMA-*g*-3ABA/MWCNTs/CPE towards reduction of H_2O_2 was first investigated by CV (Fig. 9). When H_2O_2 was added in the solution, there was a disappearance of the oxidation peak and an increase of the reduction peak depending on the concentration of H_2O_2 in solution. This result confirms that Hb adsorbed on PSMA-*g*-3ABA/MWCNTs/CPE had a pseudo peroxidase activity. A possible mechanism of reaction of H_2O_2 catalyzed by the Hb-PSMA-*g*-3ABA/MWCNTs/CPE is postulated as follows:

$$[\mathrm{HbFe(III)}] + \mathrm{H^+} + \mathrm{e^-} \leftrightarrow [\mathrm{HbFe(II)}]$$

$$2[\mathrm{HbFe(II)}] + \mathrm{H_2O_2} + 2\mathrm{H^+} + 2\mathrm{e^-} \leftrightarrow 2[\mathrm{HbFe(III)}] + 2\mathrm{H_2O}$$

According to above proposed mechanism, HbFe(II) generated on the electrode was chemically oxidized by H_2O_2, and the produced HbFe(III) was reduced again at the electrode in a catalytic cycle. When increasing the H_2O_2 concentration, more and more HbFe(II) was chemically oxidized, resulting in an increase of the HbFe(III) reduction peak and a decrease of the HbFe(II) oxidation peak.

Electrocatalytic reductions of H_2O_2 were performed by amperometric current–time method, which is one of the most frequently used techniques for biosensor. Fig. 10 shows the amperometric responses of different concentrations of H_2O_2 at Hb-PSMA-*g*-3ABA/MWCNTs/CPE with an applied potential of −0.4 V vs. Ag|AgCl|KCl (3.0 M) in 0.1 M PBS (pH 7.0). From the steady-state current response of H_2O_2 at the modified electrode, this proposed electrode achieved 95% of the steady-state current within 5 s. It implies that the Hb-PSMA-*g*-3ABA/MWCNTs/CPE might provide a favorable microenvironment for studying the fast electrode process kinetics. The reduction currents are proportional to the concentration of H_2O_2 ranging from 1.0×10^{-6} to 5×10^{-4} M (inset of Fig. 10), with a regression equation of I_p (μA) = −0.57–0.21 C (μM) ($R^2 = 0.9989$). The detection limit is calculated to be 3.2×10^{-7} M (S/N = 3). Table 1 compares the performance of the Hb-PSMA-*g*-3ABA/MWCNTs/CPE with the other sensors for electrochemical determination of H_2O_2 reported in the literature, demonstrating that the obtained results from the present electrode are comparable with other modified electrodes for determination of H_2O_2.

Kamin and Wilson [63] suggested that an enzymatic reaction is catalytically controlled, and an apparent Michaelis–Menten constant (K_m) can be calculated for the immobilized enzyme by the amperometric method. The Lineweaver–Burk [64] equation is as follows:

$$(1/i_{ss}) = (1/i_{max}) + (K_m/i_{max}C) \quad (1)$$

where i_{ss} is the steady-state current after the addition of substrate, i_{max} is the maximum current under saturated substrate conditions, and C is the substrate concentration. K_m can be obtained from the slope and the intercept of the plot. Therefore, the K_m value for this Hb-PSMA-*g*-3ABA/MWCNTs/CPE is calculated to be 0.22 mM. This value for apparent Michaelis–Menten constant is smaller than the apparent Michaelis–Menten constant of hemoglobin at Hb/graphene/chitosan 0.344 mM [65], Hb/AuNPs/PDDA-G 0.57 mM [66], Hb/$PEO_{20}PO_{70}EO_{20}$ (P123) 0.51 mM [67], and Hb/PHD/MWCNTs 0.51 mM [30]. It is reasonable to think that PSMA-*g*-3ABA/MWCNTs nanocomposite provides a friendly microenvironment to retain Hb's bioactivity. In addition, the porous structure of PSMA-*g*-3ABA/MWCNTs/CPE provides a significant increase in the effectiveness for Hb loading on the electrode surface, decreasing the reorganizational energy for electron transfer and allowing the electroactive probe to easily diffuse through the films.

3.5. Interference study

A possible interference of some substances that might occur in real samples was evaluated. The interfering substance was added to the PBS containing 10 μM H_2O_2. No significant interference could be observed formatters, such as 60 μM of glucose, acetic acid, ethanol, L-cysteine, L-tyrosine glycin citric acid, SO_4^{2-}, CO_3^{2-}, ClO_3^-, Cl^-, Br^-, and I^- (signal change below 4%), indicating that these compounds did not affect the determination of H_2O_2. In order to prove the reliability of the proposed biosensor for H_2O_2 detection, we applied the modified electrode to the determination of H_2O_2 in spiked rain water samples. The obtained results are given in Table 2. The R.S.D. % and recovery calculations indicate the potential practical application of our proposed biosensor for H_2O_2 in real samples.

3.6. Stability and reproducibility of the Hb-PSMA-g-3ABA/MWCNTs/CPE

The stability of Hb-PSMA-*g*-3ABA/MWCNTs/CPE was investigated. The biosensor could retain the direct electrochemistry of the immobilized Hb at constant current values upon the continuous CV sweep over the potential range from −0.7 V to 0.0 V at 100 mV s^{-1}, suggesting that Hb can tightly adsorb on the surface of PSMA-*g*-3ABA/MWCNTs/CPE. When stored at 4 °C for over 2 weeks, the biosensor retained 90% of the initial sensitivity to H_2O_2. The relative standard deviation (R.S.D.) of the biosensor is 1.43% for 10 successive determinations in 1×10^{-4} M H_2O_2 solution, indicating a good precision. The

Table 1
The performances of the different modified electrodes for determination of H_2O_2.

Electrode	Modifier	pH	Linear range (μM)	LOD (μM)	Reference
Glassy carbon	Poly(lactic-co-glycolic acid)/ionic liquid	7.0	5.0–8050.0	0.237	[60]
Glassy carbon	Poly(acrylonitrile-*co*-acrylic acid)	7.0	9.2–2000.0	4.5	[45]
Glassy carbon	Poly(ε-caprolactone)	7.0	2.0–30.0	6.07	[61]
Gold electrode	Poly-allylamine	7.0	2.5–500.0	0.2	[62]
Glassy carbon	PHEMA-b-DMAEMA/MWCNTs	7.0	1.0–1500.0	0.35	[30]
Pyrolytic graphite	Triblock copolymer $EO_{20}PO_{70}EO_{20}$ (P123)	6.0	1–500.0	0.5	[66]
Glassy carbon	Poly(diallyldimethylammonium chloride)/gold nanoparticles/graphene	7.4	6.0–1010.0	0.39	[67]
Carbon paste	PSMA-g-3ABA/MWCNTs	7.0	1.0–500.0	0.32	This work

Table 2
The results of analysis of H_2O_2 in rain water sample.

Sample	Added (μM)	Found (μM)	Recovery	R.S.D. (%)
Rain water	0.0	0.0	–	–
	20.0	19.8	99.0	4.3
	30.0	30.2	100.6	5.2
	80.0	81.1	101.3	3.8
	120.0	120.4	100.3	2.1

results demonstrated that PSMA-*g*-3ABA/MWCNTs nanocomposite film was a suitable matrix for immobilization of Hb to retain its activity and prevent it from leaking out of the film.

4. Conclusions

A simple method was developed for the effective immobilization of Hb by the construction of PSMA-*g*-3ABA/MWCNTs nanocomposite. This kind of nanocomposite film provided a favorable microenvironment around Hb to retain its biological activity and native structure. Moreover, the biosensor based on the PSMA-*g*-3ABA/MWCNTs nanocomposite film modified electrodes exhibited good electrocatalytical response to the reduction of H_2O_2 with fast response, good reproducibility and stability. Hence, it provides a promising application for copolymer materials with low electrical conductivity for the study of direct electron transfer of proteins and the development of third generation biosensors.

References

[1] M.F. Bergamini, D.P. Santos, M.V.B. Zanoni, J. Electroanal. Chem. 690 (2013) 47–52.
[2] S. Tajik, M.A. Taher, H. Beitollahi, Sensors Actuators B 188 (2013) 923–930.
[3] A. Mokhtari, H. Karimi-Maleh, A.A. Ensafi, H. Beitollahi, Sensors Actuators B 169 (2012) 96–105.
[4] M. Mazloum-Ardakani, H. Beitollahi, M.K. Amini, F. Mirkhalaf, M. Abdollahi-Alibeik, Sensors Actuators B 151 (2010) 243–249.
[5] J.B. Raoof, R. Ojani, H. Beitollahi, Electroanalysis 19 (2007) 1822–1830.
[6] J.B. Raoof, R. Ojani, H. Beitollahi, R. Hossienzadeh, Electroanalysis 18 (2006) 1193–1201.
[7] H. Beitollahi, J.B. Raoof, R. Hosseinzadeh, Electroanalysis 23 (2011) 1934–1940.
[8] D. Shan, E. Han, H. Xue, S. Cosnier, Biomacromolecules 8 (2007) 3041–3046.
[9] F.A. Armstrong, H.A.O. Hill, N.J. Walton, Acc. Chem. Res. 21 (1998) 407–413.
[10] X.C. Li, W. Zheng, L.M. Zhang, P. Yu, Y.Q. Lin, L. Su, L.Q. Mao, Anal. Chem. 81 (2009) 8557–8563.
[11] Q. Wang, W. Xu, P. Wu, H. Zhang, C.X. Cai, B. Zhao, J. Phys. Chem. B 114 (2010) 12754–12764.
[12] A. Ahmad, M.S. Akhtar, V. Bhakuni, Biochemistry 40 (2001) 1945–1955.
[13] D.M. Gouda, S.A. Singh, A.G.A. Rao, M.S. Thakur, N.G. Karanth, J. Biol. Chem. 278 (2003) 24324–24333.
[14] M. Baghayeri, E. Nazarzadeh Zare, M. Mansour Lakouraj, Biosens. Bioelectron. 55 (2014) 259–265.
[15] M. Baghayeri, E. Nazarzadeh Zare, M. Namadchian, Sensors Actuators B 188 (2013) 227–234.
[16] P. Mailley, E.A. Cummings, S.C. Mailley, B.R. Eggins, E. McAdams, S. Cosnier, Anal. Chem. 75 (2003) 5422–5428.
[17] R. Renneberg, G. Trott-Kriegeskorte, M. Lietz, V. Ja¨ger, M. Pawlowa, G. Kaiser, U. Wollenberger, F. Schubert, R. Wagner, R.D. Schmid, F.W. Scheller, J. Biotechnol. 21 (1991) 173–186.
[18] N. Yoshida, K. Yano, T. Morita, S.J. McNiven, H. Nakamura, I. Karube, Analyst 125 (2000) 2280–2284.
[19] Y. Morita, H. Saino, K. Tojo, Biol. Pharm. Bull. 21 (1998) 72–75.
[20] A. Dankwardt, J. Muller, B. Hock, Anal. Chim. Acta. 362 (1998) 35–45.
[21] V.B. Kushwaha, J. Appl. Polym. Sci. 74 (1999) 3469–3472.
[22] P.M. Ajayan, J.M. Tour, Nature 447 (2007) 1066–1068.
[23] D.W. Schaefer, R.S. Justice, Macromolecules 40 (2007) 8501–8517.
[24] M.T. Byrne, Y. Gun'ko, Adv. Mater. 22 (2010) 1672–1688.
[25] C. Li, E.T. Thostenson, T.-W. Chou, Compos. Sci. Technol. 68 (2008) 1227–1249.
[26] T. Villmow, S. Pegel, A. John, R. Rentenberger, P. Ptschke, Mater. Today 14 (2011) 340–345.
[27] B. Kumar, J.-F. Feller, M. Castro, J. Lu, Talanta 81 (2010) 908–915.
[28] S. Liu, B. Lin, X. Yang, Q. Zhang, J. Phys. Chem. B 111 (2007) 1182–1188.
[29] Y. Wen, H. Wu, S. Chen, Y. Lu, H. Shen, N. Jia, Electrochim. Acta 54 (2009) 707–708.
[30] Z. Wang, J. Yi, S. Yang, Sensors Actuators B 176 (2013) 211–216.
[31] L.L. Ma, P. Jie, S.S. Venkatraman, Adv. Funct. Mater. 18 (2008) 716–725.
[32] J.D. Clapper, M.E. Pearce, C.A. Guymon, A.K. Salem, Biomacromolecules 9 (2008) 1188–1194.
[33] L. Wang, X. Zhang, H. Xiong, S. Wang, Biosens. Bioelectron. 26 (2010) 991–995.
[34] E. Nazarzadeh Zareh, P. Najafi Moghadam, J. Appl. Polym. Sci. 122 (2011) 97–104.
[35] P. Najafi Moghadam, E. Nazarzadeh Zareh, E-polymers 54 (2010) 1–9.
[36] P. Najafi Moghadam, E. Nazarzadeh Zareh, H. Amiri, M. Mansour Lakouraj, Compos. Interfaces 19 (2012) 475–488.
[37] P. Najafi Moghadam, E. Azaryan, B. Zeynizade, J. Macromol. Sci. Pure Appl. Chem. 47 (2010) 839–848.
[38] R. Hasanzadeh, P. Najafi Moghadam, N. Samadi, Polym. Adv. Technol. 24 (2013) 34–41.
[39] R. Hasanzadeh, P. Najafi Moghadam, N. Samadi, S. Asri-Rezaei, J. Appl. Polym. Sci. 127 (4) (2013) 2875–2883.
[40] P. Najafi Moghadam, R. Hasanzadeh, J. Khalafy, Iran. Polym. J. 22 (2013) 133–142.
[41] J.B. Raoof, R. Ojani, M. Baghayeri, M. Amiri-Aref, Anal. Methods 4 (2012) 1579–1587.
[42] E. Laviron, J. Electroanal. Chem. 100 (1979) 263–270.
[43] E. Laviron, J. Electroanal. Chem. 101 (1979) 19–28.
[44] J.J. Xu, H.Y. Chen, Anal. Biochem. 280 (2000) 221–226.
[45] D. Shan, G. Cheng, D. Zhu, H. Xue, S. Cosnier, S. Ding, Sensors Actuators B 137 (2009) 259–265.
[46] X. Lu, J. Hu, X. Yao, Z. Wang, J. Li, Biomacromolecules 7 (2006) 975–980.
[47] J.H. Shi, B.X. Yang, S. Hong Goh, Eur. Polym. J. 45 (2009) 1002–1008.
[48] Y. Wen, H. Wu, S. Chen, Y. Lu, H. Shen, N. Jia, Electrochim. Acta 54 (2009) 7078–7084.
[49] C.X. Cai, J. Chen, Anal. Biochem. 325 (2004) 285–292.
[50] W. Zheng, Y.F. Zheng, Electrochem. Commun. 9 (2007) 1619–1623.
[51] J.J. Gooding, R. Wibowo, J. Liu, W. Yang, D. Losic, S. Orbons, F.J. Mearns, J.G. Shapter, D.B. Hibbert, J. Am. Chem. Soc. 125 (2003) 9006–9007.
[52] A.M. Bond, Modern Polarographic Methods in Analytical Chemistry, Marcel Dekker, New York, 1980. 27.
[53] H.H. Liu, Z.Q. Tian, Z.X. Lu, Z.L. Zhang, M. Zhang, D.W. Pang, Biosens. Bioelectron. 20 (2004) 294–304.
[54] Y. Li, X. Zeng, X. Liu, X. Liu, W. Wei, S. Luo, Colloids Surf, B: Biointerfaces 79 (2010) 241–245.
[55] H.L. Qi, C.X. Zhang, X.R. Li, Sensors Actuators B 114 (2006) 364–370.
[56] L. Chen, G.X. Lu, Sensors Actuators B 121 (2007) 423–429.
[57] S.Z. Zong, Y. Cao, H.X. Ju, Electroanalysis 19 (2007) 841–846.
[58] P. George, G. Hanania, Biochem. J. 55 (1953) 236–243.
[59] S.F. Wang, Z. Zhang, X.C. Shen, Z.X. Lu, D.W. Pang, K. Wong, Langmuir 21 (2005) 9260–9266.
[60] Y. Zhang, X. Sun, N. Jia, Sensors Actuators B 157 (2011) 527–532.
[61] W. Zheng, J. Li, Y.F. Zheng, Biosens. Bioelectron. 23 (2008) 1562–1566.
[62] A.K.M. Kafi, D.-Y. Lee, S.-H. Park, Y.-S. Kwon, Thin Solid Films 515 (2007) 5179–5183.
[63] R.A. Kamin, G.S. Wilson, Anal. Chem. 52 (1980) 1198–1205.
[64] J. Li, S.N. Tan, H. Ge, Anal. Chim. Acta. 335 (1996) 137–145.
[65] H. Xu, H. Dai, G. Chen, Talanta 81 (2010) 334–338.
[66] N. Jia, Q. Lian, Z. Wang, H. Shen, Sensors Actuators B 137 (2009) 230–234.
[67] Q. Feng, K. Liu, J. Fu, Y. Zhang, Z. Zheng, C. Wang, Y. Du, W. Ye, Electrochim. Acta 60 (2012) 304–308